SARS-CoV-2 induces a unique mitochondrial transcriptome signature

Brendan Miller
University of Southern California https://orcid.org/0000-0002-7461-7973
Ana Silverstein
University of Southern California
Melanie Flores
University of Southern California
Wang Xiang
University of Southern California
Kevin Cao
University of Southern California
Hiroshi Kumagai
University of Southern California
Hemal H. Mehta
University of Southern California
Kelvin Yen
University of Southern California
Su-Jeong Kim
University of Southern California
Pinchas Cohen (hassy@usc.edu)
University of Southern California https://orcid.org/0000-0002-0035-8366

Keywords: mitochondria, SARS-CoV-2, metabolism, RNASeq

DOI: https://doi.org/10.21203/rs.3.rs-36568/v1

Abstract

SARS-CoV-2 has challenged global healthcare systems in part because its clinical manifestations are heterogeneous. Variable symptoms of SARS-CoV-2 could be attributed to the virus' ability to mildly induce an innate immune response, as prior transcriptomic data has suggested. Mitochondrial dynamics might partially mediate the effect of SARS-CoV-2 on innate immunity. Many proteins encoded by SARS-CoV have been shown to localize to mitochondria and inhibit Mitochondrial Antiviral Signaling protein (MAVS). We analyzed multiple publicly available RNASeq data in order to unravel the metabolic and mitochondrial transcriptome signature of SARS-CoV-2 in primary cells, cell lines, and clinical samples (i.e., BALF and lung). We report here that SARS-CoV-2 does not dramatically regulate (1) mitochondrial-gene expression or (2) MAVS expression, but (3) downregulates nuclear-encoded mitochondrial (NEM) genes related to cellular respiration and Complex 1 assembly. We also report cell-specific and tissue-specific effects of SARS-CoV-2 on the mitochondrial-encoded and NEM transcriptome that could inform future experimental paradigm selection.

Introduction

The emergence of SARS-CoV-2 in late 2019 (COVID19) has put enormous pressure on global economic and health systems.[1] SAS-CoV-2 patients present differing degrees of disease severity due to underlying comorobidites.[2] Diabetic patients hospitalized in New York City were more likely to receive severe intensive care interventions than patients without diabetes.[3] It is unclear how certain metabolic conditions increase mortality in SARS-COV-2 patients. However, SARS-CoV-2 induces a modest pro inflammatory response that is distinct from other respiratory viruses.[4] This SARS-CoV-2 muted proinflammatory response is a phenomenon that might explain why individuals without metabolic comorbidities typically present less severe symptoms compared to patients with underlying comorbidities.

The effects of SARS-CoV-2 on the host cell innate immune response could be mediated by mitochondrial dynamics. Independent analyses of the SARS-CoV-2 transcriptomic data set revealed enrichment for mitochondrial organization processes, and host cell innate immunity is regulated by the Mitochondrial Antiviral Signaling protein (MAVS).[5,6] MAVS normally interacts with MFN2 under resting conditions.[7] But after viral infection, mitochondria-associated ER membranes and nearby mitochondria become tethered by MFN2 and RIG-1, forming a complex that recruits TRIM25 and the molecular chaperone 14-3-3e into a translocon structure.[8] This translocon localizes to the mitochondrion where it binds MAVS, after which MAVS interacts with TANK binding kinase 1, IKKA, and IKKB.[9] The host cell's immune and apoptotic response is amplified when MAVS induces phosphorylation and nuclear translocation of IRF3 (Figure 2B).

SARS-CoV, which was identified in 2002 amid the international SARS outbreak, displayed MAVS-inhibiting functions. For example, RIG-1 and MDA5 were inhibited by SARS-CoV, and the SARS-CoVORF9b targeted

the mitochondrial-associated adaptor molecule MAVS signalosome.[10] Notably, ORF9b of the novel SARS-CoV-2 has been characterized as one of the largest hubs in interactome analysis.[11] SARS-CoVOR3b also localized to the mitochondria *in vitro*, and mitochondrial-gene expression was upregulated in peripheral blood mononuclear cells (PBMC) of infected patients.[12] The interaction between SARS-CoV and mitochondria suggest that the mitochondrion also participates in the SARS-COV-2-specific host cell response. It is plausible that SARS-CoV-2 has specific effects on both the nuclear-encoded mitochondrial (NEM) transcriptome mitochondrial transcriptome and mitochondrial-encoded transcriptome. In the following analyses, we assessed the effect of SARS-CoV-2 on the mitochondrial genetic network transcriptome by reanalyzing publicly available RNASeq data.

Results

Selection of COVID datasets

In order to examine the NEM and mtDNA expression signature in SARS-CoV-2 infection, we utilized data sets that were uploaded to GEO (GSE147507 and GSE110551) and the BIG Data Center (CRA002390). These RNASeq data sets were derived from A549, A549 (ACE2), Calu-3, and NHBE cells as well as from SARS-CoV-2 patients' lung autopsies and bronchoalveolar lavage fluid (BALF). A549 cells were infected with seasonal influenza A virus (IAV), human orthopneumovirus (respiratory syncytial virus; RSV), human parainfluenza virus 3 (HPIV3), and SARS-CoV-2. ACE2-expressing A549 cells, Calu-3 cells, and NHBE cells were infected with SARS-CoV-2. NHBE cells were also infected with IAV. The original authors who curated the *in vitro* data infected SARS-CoV-2 in A549 cells at low and high multiplicities of infection (MOI). They found that the rate of SARS-CoV-2 replication after low MOI was comparable to the replication rate after high MOI in ACE2-expressing A549 cells.[4] The original authors also observed that low MOI SARS-CoV-2 infection stimulated a relative muted proinflammatory response, which was ablated in high MOI SARS-CoV-2 infection in ACE2-expression A549 cells. We specifically contrasted infection conditions by using low MOI SARS-CoV-2 in order to (1) stay consistent with previously published results and limit confounding effects from stoichiometry disruption of high SARS-CoV-2 components. The number of differentially expressed genes (DEGs) and NEM DEGs per biological source is listed in Table 1. Significant DEGs were filtered by an adjusted p value of 0.2.

Source	Total Samples	Total DEGS	Total Nuclear-Encoded Mitochondrial (NEM) DEGs	NEM DEGs as Percentage of Total DEGs	NEM DEGs as Percentage of NEM GO Annotations
NHBE	9	2840	313	12.7%	17.0%
A549 (ACE2)	6	3265	293	9.0%	16.1%
Calu-3	6	4219	455	10.8%	24.7%
BALF	5	5353	411	7.7%	22.3%
Lung	10	475	28	5.9%	1.6%

SARS-CoV-2 Differentially Regulates mtDNA-Encoded Genes

We hypothesized that SARS-CoV-2 infection would upregulate mtDNA-encoded gene expression due to the effects of SARS-CoV on patient PBMCs.[12] In our analyses, however, we observed minimal regulation of mtDNA-encoded genes after SARS-CoV-2 infection and – against our original hypothesis – downregulation of mtDNA-genes in BALF (Figure 1). SARS-CoV-2 infection only upregulated mt-CytB and downregulated mt-TN in primary NHBE cells, whereas IAV and IAVdNS1 (i.e., IAV with a null interferon antagonist NS1 mutant) downregulated every mtDNA-encoded protein gene and several tRNAs (Figure 1A). Such strong regulatory effects of IAV on mtDNA-encoded genes was not consistent in cancerous cell lines. In A549 cells, while IAV downregulated mt-ND6 and mt-ATP6, we did not observe the same global downregulation as we did in primary NHBE cells, and we found *16S rRNA* was upregulated only in these cancerous cells (Figure 1B). HPV did not regulate expression of any mtDNA-encoded protein gene (Figure 1B). RSV induced dramatic upregulation of every mtDNA-encoded protein along mt-rRNA and a few tRNAs (Figure 1B). SARS-CoV-2 did not upregulate any mtDNA-encoded proteins but did upregulate *16S rRNA* in Calu-3 and ACE2-expressing A549 cells (Figure 1B). In BALF, SARS-CoV-2 surprisingly downregulated nearly every mtDNA-encoded gene along with several mt-tRNAs (Figure 1C). Overall, following SARS-CoV-2 infection, we observed downregulation of mtDNA-encoded genes in BALF, which is opposite to the minimal upregulation we observed in primary and cell lines. The complete list of significant mtDNA-encoded genes and fold changes are included in Supplementary Table: mtDNA Differentially Expressed Genes.

SARS-CoV-2 Does Not Downregulate MAVS Expression

We hypothesized that MAVS expression would not be significantly downregulated after SARS-CoV-2 infection. Indeed, there were no significant effects of SARS-CoV-2 on MAVS expression in ACE2-expressing A549 cells, Calu-3 cells, NHBE cells, BALF, and lung (Figure 2A). In contrast, IAV, RSV, and HPIV all induced a statistically significant downregulation of MAVS. IAV-infected A549 cells induced the most dramatic downregulation of MAVS (Log2FC = -0.98; Padj = 1.32E-08), followed by IAVdNS1 in NHBE cells (Log2FC = -0.93; Padj = 5.35E-04), IAV in NHBE cells (Log2FC = -0.52; Padj = 1.11E-01), RSV in A549 cells (Log2FC = -0.33; Padj = 7.00E-02) and HPIV in A549 cells (Log2FC = -0.20; Padj = 2.02E-01).

NEMS Sufficiently Classifies SARS-CoV-2

Given that MAVS and mtDNA-encoded gene expression differs among SARS-CoV-2, HPIV, RSV, and IAV, we hypothesized that the global NEM signature would sufficiently classify SARS-CoV-2. Therefore, we conducted a principal component analysis (PCA) exclusively on an NEM-extracted gene set. As expected, the first two principal components sufficiently reduced NEM expression variance in a manner that classified SARS-CoV-2 in primary cells, cell lines, and clinical samples (Figure 3). The amount of variance that the first two NEM-specific two principal components explain total 81%, 60%, and 56% for primary cells, cell lines, and clinical samples, respectively.

SARS-CoV-2 Specific NEM-Enriched Pathways

Since we showed that NEMs are sufficient to classify SARS-CoV-2, HPIV, RSV, and IAV, we attempted to unravel the biological processes that these NEMs modify. All NEMs were extracted from the complete list of statistically significant DEGs. Hierarchical clustering of NEMs showed distinct signatures by viral infection (Figure 4A). We then then conducted gene enrichment analyses by inputting this set of significant NEMs against a universe background of all total significant DEGs. Four separate gene enrichment analyses were conducted (i.e., primary cells, cell lines, BALF, and lung).

The GO enriched terms of small molecule metabolism, phosphorus metabolism, oxidation-reduction, and cellular amide metabolism were all shared between SARS-CoV-2 and IAV in NHBE primary cells (Figure 4B; filtered by >20% NEM within gene set). SARS-CoV-2 particularly induced greater enrichment for mitochondrion organization and catabolism compared to IAV and IAVdNS1 (Figure 4B). Furthermore, the top 10 most significant enriched for SARS-CoV-2 mapped back to mitochondrial translation, mitochondrial organization, and cellular respiration (Figure 4C and 4D). SARS-CoV-2 not only induced global downregulation of the metabolic pathways shown in Figure 4C (Log2FC), but the degree of downregulation was greatest in SARS-CoV-2, as illustrated in the right panel of Figure 4C with hierarchical clustering scores colored (SARS-CoV-2 Score). Several mitochondrial ribosome protein genes (e.g., MRPL55, MRPL47, MRPL42, etc.) and Complex 1 related genes (e.g., NDUFB11, NDUFB2, NDUFC1, etc.) were expressed much less after SARS-CoV-2 compared to IAV and IAVdNS1 (Figure 4C and 4D).

In cell lines, as we noted in primary cells, enrichment for oxidation-reduction metabolism was shared among all viral infections (i.e., SARS-CoV-2, HPIV, RSV, and IAV). Hierarchical clustering showed distinct NEM signatures by viral infection (Figure 5A). For SARS-CoV-2 in ACE2-expressing A549 cells, we observed more NEMs involved in catabolism and small molecule metabolism, but we did not observe this same degree of enrichment in Calu-3 cells (Figure 5B). In addition, Calu-3 cells contained more NEMs enriched for mitochondrion organization than in ACE2-expressing A549 cells. We still observed reduced expression of mitochondrial Complex 1 related genes (e.g., NDUFS2, NDUFB7, NDUFS6, etc.) after SARS-CoV-2 compared to IAV, HPIV, and RSV IAVdNS1 (Figure 5D). Notably, unlike the downregulation of mitochondrial ribosome protein genes in primary cells, we did not observe similar enrichment for mitochondrial translation after SARS-CoV-2 infection. Instead, a greater number of differentially expressed genes related to carboxylic acid metabolism (FASN, ACAT1, ACAT2, etc.) were observed in cell lines after SARS-CoV-2 infection.

The top 10 most significant enriched processes after SARS-CoV-2 in ACE2-expressing A549 cells mapped back to cellular respiration, oxidation-reduction, small molecule metabolism, among many other interrelated metabolic pathways (Figure 5C). As we observed in primary

NHBE cells, we found similar downregulation of genes mapping back to cellular respiration and mitochondrion organization after SARS-CoV-2 infection. Additionally, while we observed downregulation of catabolic genes after SARS-CoV-2 infection, the degree of downregulation relative to other viruses was not as great (i.e., some NEMs were expressed at greater levels after SARS-CoV-2 compared to other viruses), which is in conflict to that observed in primary cells (i.e., Figure 5C SARS-CoV-2 Score shows positive scores for genes that are downregulated by log 2 fold change). We also observed greater expression of PINK1 after SARS-CoV-2 infection in ACE2-expressing cells, suggesting differential mitochondrial dynamics specific to cell lines. Upregulation of PINK1 could explain why we a greater catabolic gene set percentage in SARS-CoV-2 compared to other viruses. Overall, we also observed attenuation of cellular respiration, oxidation-reduction, and related interconnected pathways in cell lines after SARS-CoV-2 infection relative to IAV, HPIV, and RSV.

BALF and lung clinical samples also contained downregulation of genes involved in cellular respiration and Complex 1 assembly after SARS-CoV-2 infection (BALF: NDUFAF6, NDUFB9, NDUFV2, etc.; Lung: NDUFB1, NDUFB7, NDUFAL2). However, the effect of SARS-CoV-2 on the NEM transcriptome was not as dramatic in lung compared to BALF. In BALF, the most significant NEM-enriched included orhanophosphate metabolism, mitochondrial gene expression, cellular respiration, oxidation-reduction, etc. (Figure 6A-B). The majority of these genes downregulated after SARS-CoV-2 infection, which was similar to the signature in primary cells and cell lines. In lung, despite identifying just 28 significant NEMs, mitochondrion organization, phosphorus metabolism, and overall energy metabolism were enriched (Figure 6C-D).

Generally, across cellular and clinical samples, several metabolic pathways were enriched after viral infection, but the SARS-CoV-2-specific signature included downregulation of NEMs involved in cellular respiration and Complex 1 assembly (NDUF family of proteins). Mitochondrial ribosome gene expression was particularly downregulated after SARS-CoV-2 infection in primary cells (greater downregulation compared to IAV) and clinical samples, although we did not observe this similar mitochondrial translation signature in cell lines. There were clear tissue and cell-specific differences across all analyses related to oxidation-

reduction, small molecule metabolism, and carboxylic metabolism, suggesting SARS-CoV-2 may affect metabolism differently per cell type.

Discussion

We concentrated on the mitochondrial and nuclear-encoded mitochondrial gene host response to SARS-CoV-2 and other human respiratory viruses in multiple cell models and clinical samples. Our analyses showed that the metabolic transcriptome signature of SARS-CoV-2 infection included both shared and independent biological processes to IAV, HPIV, and RSV. We observed three notable metabolic transcriptomic signature differences including mitochondrial-gene expression, MAVS expression, and NEM biological processes.

First, we found that SARS-CoV-2 did not induce a dramatic mitochondrial-gene expression signature in NHBE, A549, and Calu-3 cells. In NHBE cells, we observed that IAV and IAVdNS1 induced near global downregulation of mitochondrial-encoded genes, including all 13 protein-encoding genes. Since IAVdNS1 (i.e., IAV without its interferon antagonizing protein NS1) also induced similar downregulation of mitochondrial-encoded genes as IAV, it is plausible that these mitochondrial-gene regulatory effects are independent from an interferon response. Furthermore, since SARS-CoV-2 did not drastically influence mitochondrial-gene expression, this suggests (1) cells are not experiencing extreme energetic stress, (2) capacity for SARS-CoV-2 to evade mechanisms regulating mitochondrial-gene expression, or (3) compensation via the NEM network.

We did, however, observe dramatic downregulation of mitochondrial-gene expression in human BALF after SARS-CoV-2 infection, although we did not observe the same degree of downregulation in human lung. The cellular profile of BALF after infection differs significantly compared to resting state conditions. Prior reports have showed nearly a 900-fold increase in neutrophil infiltration after LPS stimulation.[13] Therefore, it is possible that decrease in mitochondrial-gene expression that we observed in SARS-CoV-2 patient BALF is a byproduct of a different cellular profile, and it is also possible that SARS-CoV-2 affects mitochondria in immune cells differently than in lung cells. Furthermore, we are able to quantify expression mitochondrial-encoded genes in this traditional RNASeq workflow, but we cannot rule out that the effects we observed are partially influenced by RNA with non-protein-encoding functions. Perhaps the differences (or lack thereof) in mitochondrial-gene expression are a byproduct of mitochondrial small open reading frame post-transcriptional regulation or the immune-signaling capacity of mitochondrial RNA and DNA released into the cytoplasm.[14-16]

Second, we found that SARS-CoV-2 did not alter MAVS expression, whereas IAV, HPIV, and RSV all decreased MAVS expression. Although SARS-CoV-2 differentially regulates the host cell's interferon response, MAVS is not directly regulated by interferons.[17] MAVS is instead regulated by a negative feedback loop by reactive oxygen species (ROS).[18] MAVS expression typically decreases after RNA viral infection due to the rise of ROS.[19] MAVS is also regulated by calcium, ATP, cholesterol, ceramides, and

phospholipids.[20] That SARS-CoV-2 does not affect MAVS expression suggests (1) SARS-CoV-2 may be capable of “hijacking” MAVS; (2) in the presence of SARS-CoV-2, MAVS is regulated differentially at the post-transcriptional or post-translational level; or (3) SARS-CoV-2 can propagate efficiently in the presence of unaltered MAVS expression, which could partially explain the muted antiviral response published previously.

Third, we observed that, across multiple cell and tissue types, SARS-CoV-2 reduced NEM expression related to cellular respiration and Complex 1 assembly. Reports on respiratory viruses such as RSV have indicated that Complex 1 inhibition could promote efficient viral replication.[21] We found that many NDUF Complex 1-associated proteins were downregulated after SARS-CoV-2 infection in NHBE cells, cell lines, BALF, and lung. Primary cells and BALF showed the greatest degree of downregulation of genes related to cellular respiration. SARS-CoV-2 not only decreased expression to many NDUF family of genes, but also several mitochondrial ribosome protein related genes in primary cells and BALF, observations of which did not carry over to cell lines. It is possible that the cancerous nature of A549 and Calu-3 cells limits our interpretation on metabolism due to naturally different cellular metabolic features.[22] In addition, in primary cells and cell lines, we found that SARS-CoV-2 uniquely affected a greater number of genes related to cellular catabolism, but it affected fewer genes related to cellular amide processing compared to other viruses, which could be due to the altered MAVS expression across viral infections. We also saw discordant shares of NEMs related to lipid processing and carboxylic acid metabolism across cell and tissues after SARS-CoV-2 infection perhaps due to the underlying biology of those cells. For example, we observed a greater share of NEMs related to carboxylic acid in primary cells after SARS-CoV-2 infection relative to other viruses, while, in contrast, we observed greater shares after other respiratory viral infections in cell lines.

In addition to the biological implications of SARS-CoV-2 infection presented here, our analyses suggest future research should carefully consider the *in vitro* model, especially if the desired outcome of interest is closely related to metabolic features. We highlighted more potent metabolic transcriptomic effects of SARS-CoV-2 and IAV in NHBE cells compared to A549 and Calu-3 cells. We observed several mitochondrial ribosome protein genes were downregulated after SARS-CoV-2 in NHBE cells, but we did not observe a similar phenomenon in cancerous cell lines and human BALF and lung. We found that IAV and IAVdNS1 potently downregulation mitochondrial-gene expression in primary NHBE cells but not to the same degree in A549 cells. We also identified significantly fewer overall genes and NEM genes that were differentially expressed in human lungs, which suggests tissues with heterogenous cellular profiles could be confounding and therefore hiding true metabolic effects.

Despite cell and tissue-specific effects, our analyses showed consistent downregulation of MAVS and cellular respiration was a key, shared feature of SARS-CoV-2 infection in multiple cell and tissue sources. Recent reports have predicted that SARS-CoV-2 RNA localizes to the mitochondrion.[23] An additional pre-review report hinted that it is plausible that SARS-CoV-2 RNA can anneal with mitochondrial deubuiquitanse USP30, a subunit of ubuquiting protein ligase complex FBX021 (https://www.biorxiv.org/content/10.1101/2020.04.08.031856v3.full). SARS-CoV-2 RNA acting as an

RNAi might explain many of the downregulatory expression effects that we observed. Downregulation of genes involved in cellular respiration could limit ROS production and, as a result, promote viral replication. Follow-up studies should consider the mechanisms by which SARS-CoV-2 affects mitochondrial biology. Analyses presented here have further characterized the pathogenesis of SARS-CoV-2 infection in context of mitochondrial biology and highlighted additional therapeutic directions.

Methods

The molecular preparation workflow for the RNASeq data used here has been reported previously. We downloaded sample FASTQ files from GEO or BIG Data Center. These FASTQ reads were mapped to rRNA sequences in order to remove cytoplasmic rRNA reads using STAR (v2.7.2b) with default parameters. Bioinformatically-filtered cytoplasmic rRNA FASTQ files were then mapped to the human genome (hg38) with GENCODE gene annotation (v33) using the following STAR parameters: sjdbScore 1, outFilterMultimapNmax 20, outFilterMismatchNmax 999, outFilterMismatchNoverReadLmax 0.04, alignIntronMin 20, alignIntronMax 1000000, alignMatesGapMax 1000000, and alignSJoverhangMin, alignSJDBoverhangMin 1. Aligned sorted BAM files were inputted into RR (v3.5.1) for counting. A count matrix and corresponding metadata were sorted in an S4 class derived from the *SummarizedExperiment* class of the *GenomicRanges* package in R. Count matrices were generated using the *summarizeeOverlaps* function of the *GenomicAlignemnts* package in R. Overlapping genomic features were resolved using the “Union” mode in the *summarizeOverlaps* function. Differential expression analyses were conducted using the *DESeq* R package. Significant differentially expressed genes were filtered by a padjusted value of 0.2. Genes under the “mitochondrion” Gene Ontology (GO) Term (GO:0005739) were downloaded and used for NEM enrichment analyses. There are 1842 mitochondrion GO terms, which we referred to as NEMs. This NEM gene set was used to extract such genes from the dds object generated from the DESEq2 R package. The dds object was transformed by variance stabilization using the *varianceStabilizingTrasnformation* function, which was used during the principal component analysis (*plotPCA* function in R) and euclidean heirarchial clustering (*pheatmap* function in R) scaled to each condition. Mitochondrial DNA expression heat maps were built using custom scripts in R. NEM enrichment was conducted using the *clusterProfiler* package in R. For GO analyses, the NEM-extracted gene set from statistically significant DEGs were tested against a universe background gene set of all statistically significant DEGs. This approach was implemented in order to identify biological processes that NEMS enriched compared to the background of all DEGs. The cut-off criteria for GO analysis were $p < 0.05$ and $q < 0.20$. Significant enriched terms were visualized using the two *clusterProfiler* package functions *heatplot* and *cnetplot*.

Conflict Of Interest

Pinchas Cohen is a consultant and stockholder of CohBar Inc. All other authors have no competing interests to declare.

References

1 Klompas, M. Coronavirus Disease 2019 (COVID-19): Protecting Hospitals From the Invisible. *Ann Intern Med* **172**, 619-620, doi:10.7326/M20-0751 (2020).

2 Zhong, H. *et al.* Efficacy and safety of current therapeutic options for COVID-19 - lessons to be learnt from SARS and MERS epidemic: A systematic review and meta-analysis. *Pharmacol Res*, 104872, doi:10.1016/j.phrs.2020.104872 (2020).

3 Richardson, S. *et al.* Presenting Characteristics, Comorbidities, and Outcomes Among 5700 Patients Hospitalized With COVID-19 in the New York City Area. *JAMA*, doi:10.1001/jama.2020.6775 (2020).

4 Blanco-Melo, D. *et al.* Imbalanced Host Response to SARS-CoV-2 Drives Development of COVID-19. *Cell* **181**, 1036-1045 e1039, doi:10.1016/j.cell.2020.04.026 (2020).

5 Guzzi, P. H., Mercatelli, D., Ceraolo, C. & Giorgi, F. M. Master Regulator Analysis of the SARS-CoV-2/Human Interactome. *J Clin Med* **9**, doi:10.3390/jcm9040982 (2020).

6 Sun, Q. *et al.* The specific and essential role of MAVS in antiviral innate immune responses. *Immunity* **24**, 633-642, doi:10.1016/j.immuni.2006.04.004 (2006).

7 Yasukawa, K. *et al.* Mitofusin 2 inhibits mitochondrial antiviral signaling. *Sci Signal* **2**, ra47, doi:10.1126/scisignal.2000287 (2009).

8 Liu, H. M. *et al.* The mitochondrial targeting chaperone 14-3-3epsilon regulates a RIG-I translocon that mediates membrane association and innate antiviral immunity. *Cell Host Microbe* **11**, 528-537, doi:10.1016/j.chom.2012.04.006 (2012).

9 Fang, R. *et al.* MAVS activates TBK1 and IKKepsilon through TRAFs in NEMO dependent and independent manner. *PLoS Pathog* **13**, e1006720, doi:10.1371/journal.ppat.1006720 (2017).

10 Shi, C. S. *et al.* SARS-coronavirus open reading frame-9b suppresses innate immunity by targeting mitochondria and the MAVS/TRAF3/TRAF6 signalosome. *J Immunol* **193**, 3080-3089, doi:10.4049/jimmunol.1303196 (2014).

11 Gordon, D. E. *et al.* A SARS-CoV-2-Human Protein-Protein Interaction Map Reveals Drug Targets and Potential Drug-Repurposing. *bioRxiv*, doi:10.1101/2020.03.22.002386 (2020).

12 Shao, H. *et al.* Upregulation of mitochondrial gene expression in PBMC from convalescent SARS patients. *J Clin Immunol* **26**, 546-554, doi:10.1007/s10875-006-9046-y (2006).

13 Yue, X. & Guidry, J. J. Differential Protein Expression Profiles of Bronchoalveolar Lavage Fluid Following Lipopolysaccharide-Induced Direct and Indirect Lung Injury in Mice. *Int J Mol Sci* **20**,

doi:10.3390/ijms20143401 (2019).

14 Dhir, A. *et al.* Mitochondrial double-stranded RNA triggers antiviral signalling in humans. *Nature* **560**, 238-242, doi:10.1038/s41586-018-0363-0 (2018).

15 Miller, B. *et al.* Peptides derived from small mitochondrial open reading frames: Genomic, biological, and therapeutic implications. *Exp Cell Res*, 112056, doi:10.1016/j.yexcr.2020.112056 (2020).

16 Riley, J. S. & Tait, S. W. Mitochondrial DNA in inflammation and immunity. *EMBO Rep* **21**, e49799, doi:10.15252/embr.201949799 (2020).

17 Vazquez, C. & Horner, S. M. MAVS Coordination of Antiviral Innate Immunity. *J Virol* **89**, 6974-6977, doi:10.1128/JVI.01918-14 (2015).

18 Soucy-Faulkner, A. *et al.* Requirement of NOX2 and reactive oxygen species for efficient RIG-I-mediated antiviral response through regulation of MAVS expression. *PLoS Pathog* **6**, e1000930, doi:10.1371/journal.ppat.1000930 (2010).

19 Ren, Z. *et al.* Regulation of MAVS Expression and Signaling Function in the Antiviral Innate Immune Response. *Front Immunol* **11**, 1030, doi:10.3389/fimmu.2020.01030 (2020).

20 Jacobs, J. L. & Coyne, C. B. Mechanisms of MAVS regulation at the mitochondrial membrane. *J Mol Biol* **425**, 5009-5019, doi:10.1016/j.jmb.2013.10.007 (2013).

21 Hu, M., Bogoyevitch, M. A. & Jans, D. A. Subversion of Host Cell Mitochondria by RSV to Favor Virus Production is Dependent on Inhibition of Mitochondrial Complex I and ROS Generation. *Cells* **8**, doi:10.3390/cells8111417 (2019).

22 Porporato, P. E., Filigheddu, N., Pedro, J. M. B., Kroemer, G. & Galluzzi, L. Mitochondrial metabolism and cancer. *Cell Res* **28**, 265-280, doi:10.1038/cr.2017.155 (2018).

23 Wu, K., Zou, J. & Chang, H. Y. RNA-GPS Predicts SARS-CoV-2 RNA Localization to Host Mitochondria and Nucleolus. *bioRxiv*, doi:10.1101/2020.04.28.065201 (2020).

Figures

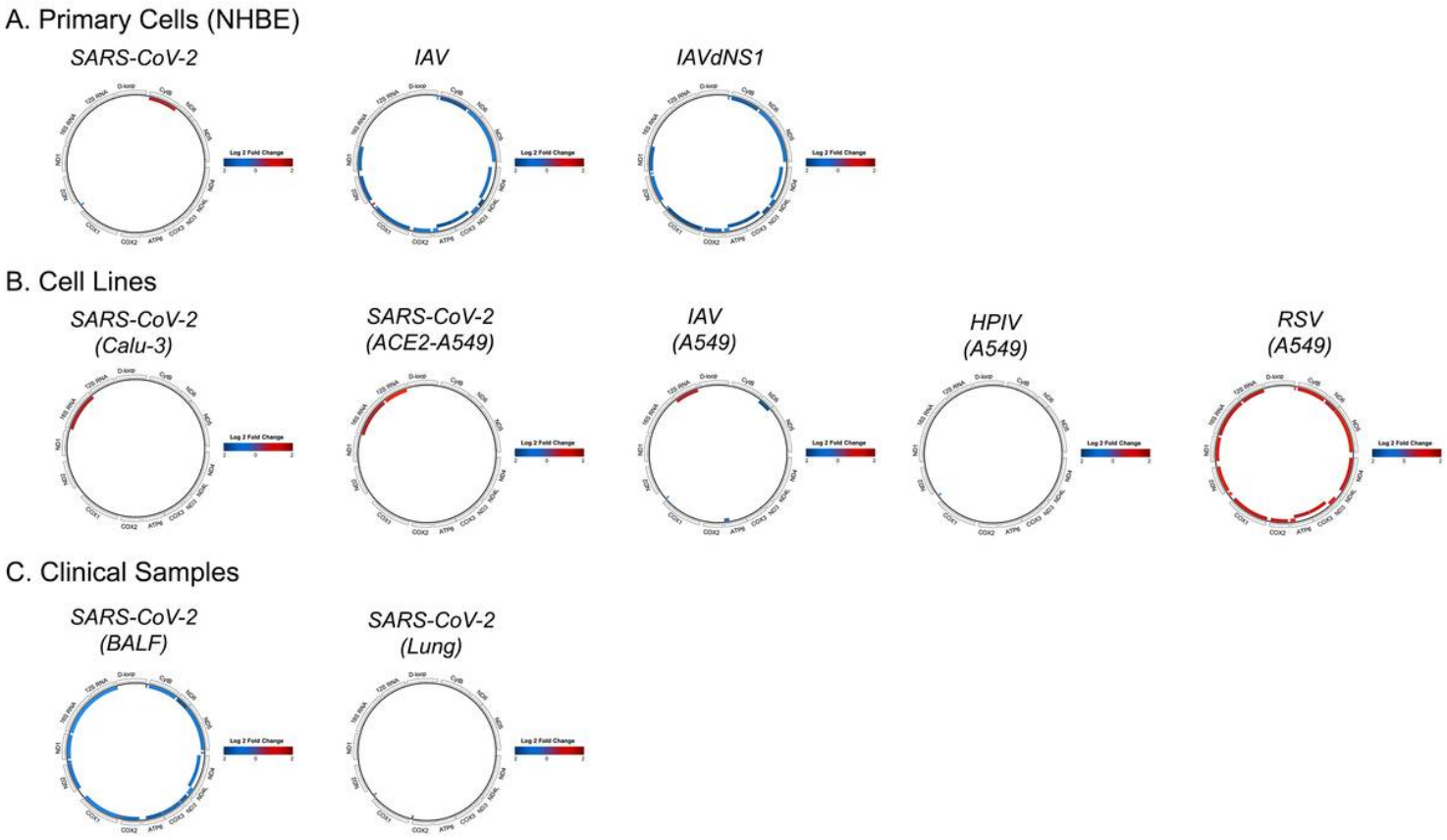

Figure 1

Mitochondrial-gene expression after viral infection in primary cells (A), cell lines (B), and clinical samples (C). Colored genes indicate log 2 fold change with a padj <0.2.

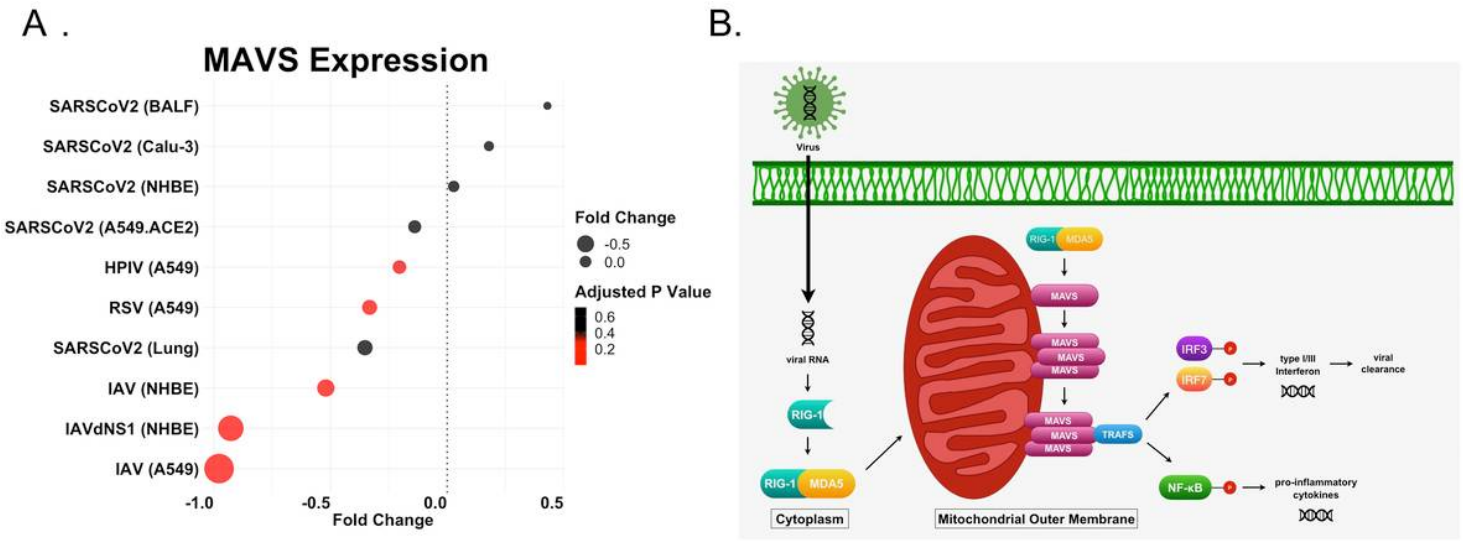

Figure 2

SARS-CoV-2 does not induce downregulation of MAVS, whereas HPIV, RSV, and IAV downregulate MAVS across cell types (A). MAVS activation leads to a type I/III interferon response with greater expression of proinflammatory cytokines (B).

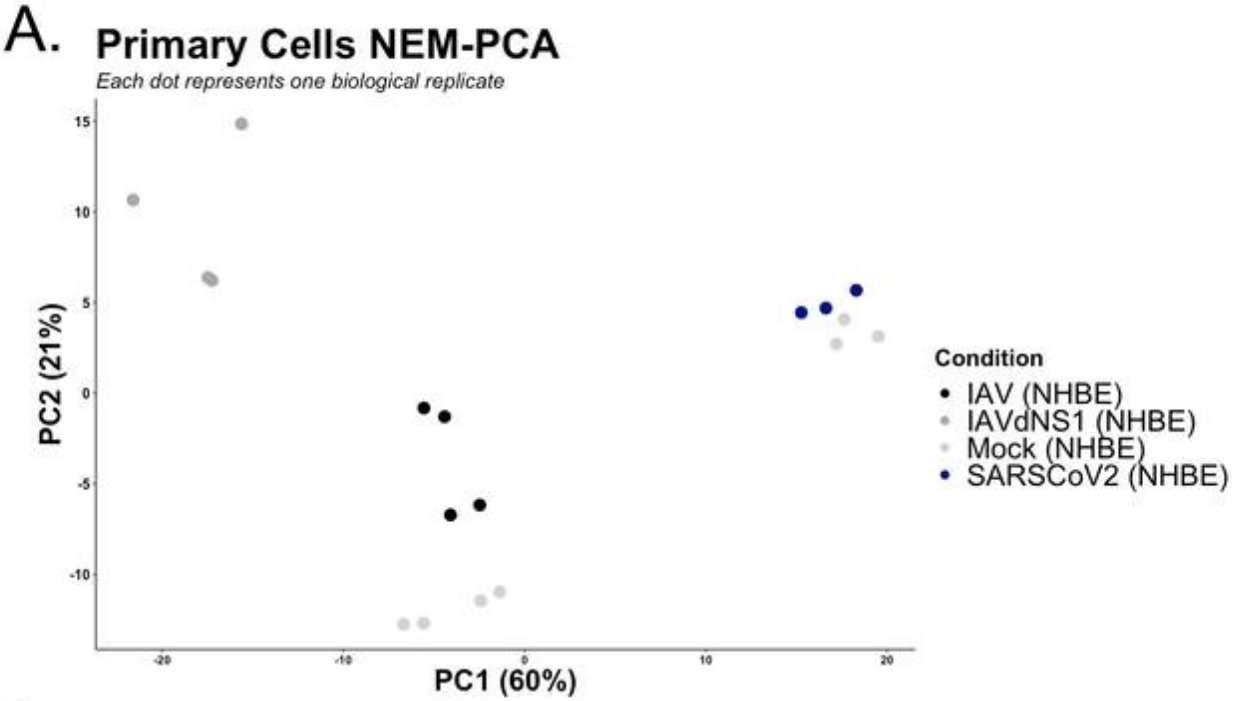
A.
Primary Cells NEM-PCA
Each dot represents one biological replicate
PC2 (21%)
PC1 (60%)
Condition
IAV (NHBE)
IAVdNS1 (NHBE)
Mock (NHBE)
SARSCoV2 (NHBE)

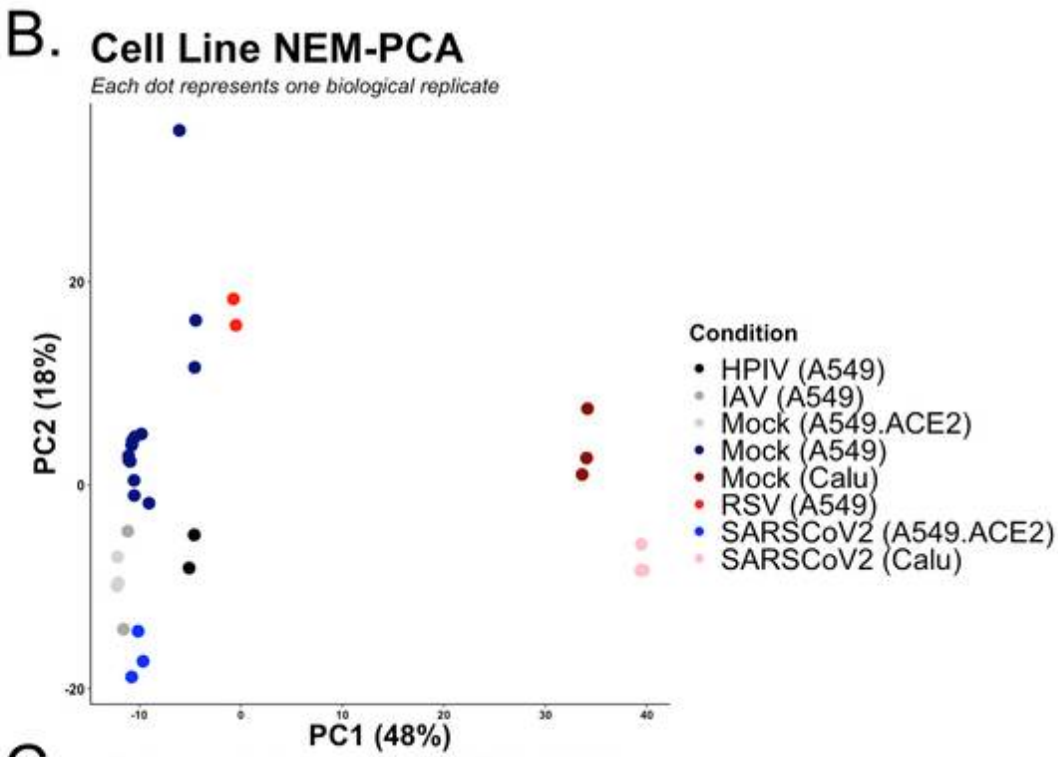
B.
Cell Line NEM-PCA
Each dot represents one biological replicate
PC2 (18%)
PC1 (48%)
Condition
HPIV (A549)
IAV (A549)
Mock (A549.ACE2)
Mock (A549)
Mock (Calu)
RSV (A549)
SARSCoV2 (A549.ACE2)
SARSCoV2 (Calu)

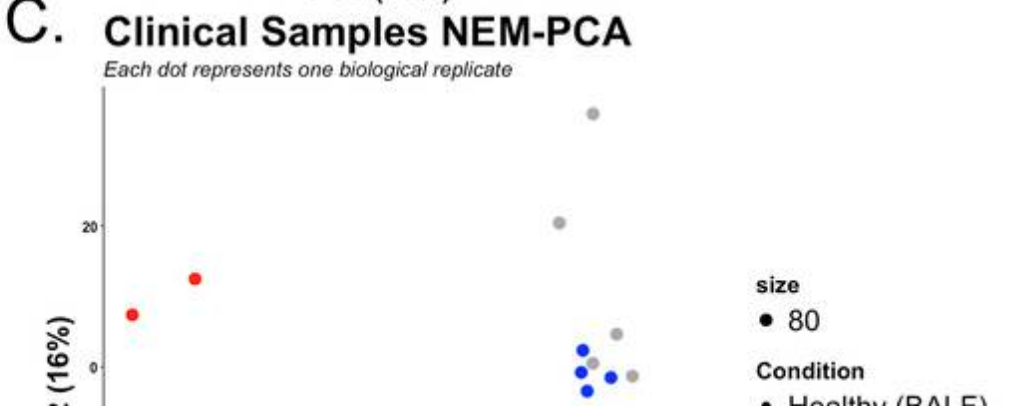
C.
Clinical Samples NEM-PCA
Each dot represents one biological replicate
size
80
Condition

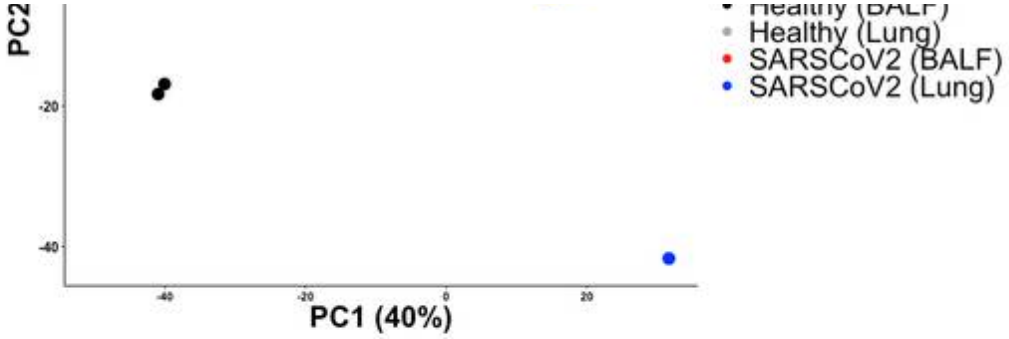

Figure 3

Principal component analysis of NEM expression data by primary cells (A), cell liens (B), and clinical samples (C).

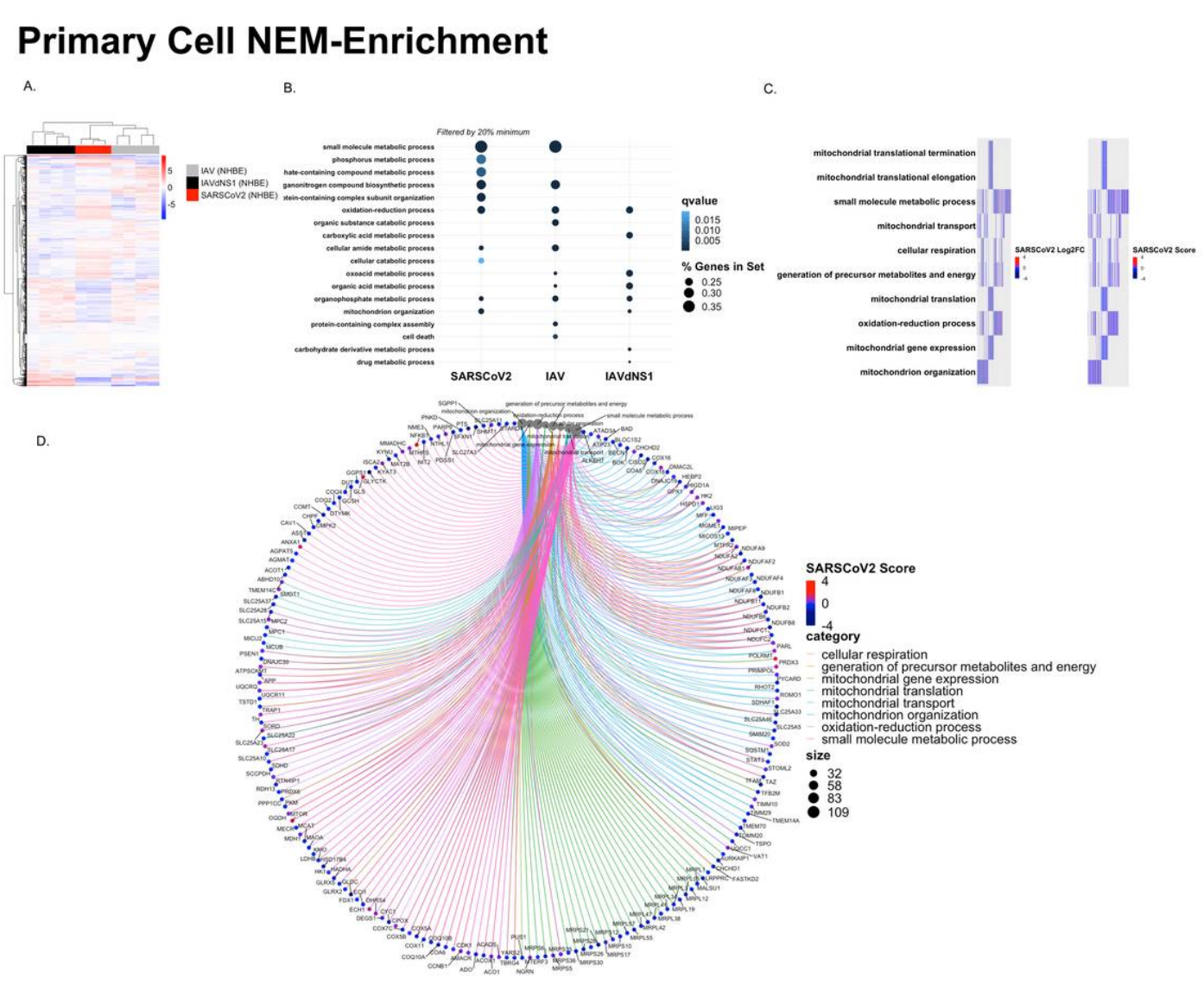

Figure 4

Biological processes affected by NEM expression. Hierarchical clustering of all NEMs separate SARS-CoV-2, IAV, and IAVdNS1 (A). Top NEM biological processes by >20% gene set enrichment (B). Top NEM biological processes by q value; left panel colors represent log 2 fold change of NEMs after SARS-CoV-2 infection and right panel represents hierarchical clustering SARS-CoV-2 scores from panel A (C). Circos plot illustrating significant NEMs and interconnectedness among biological processes.

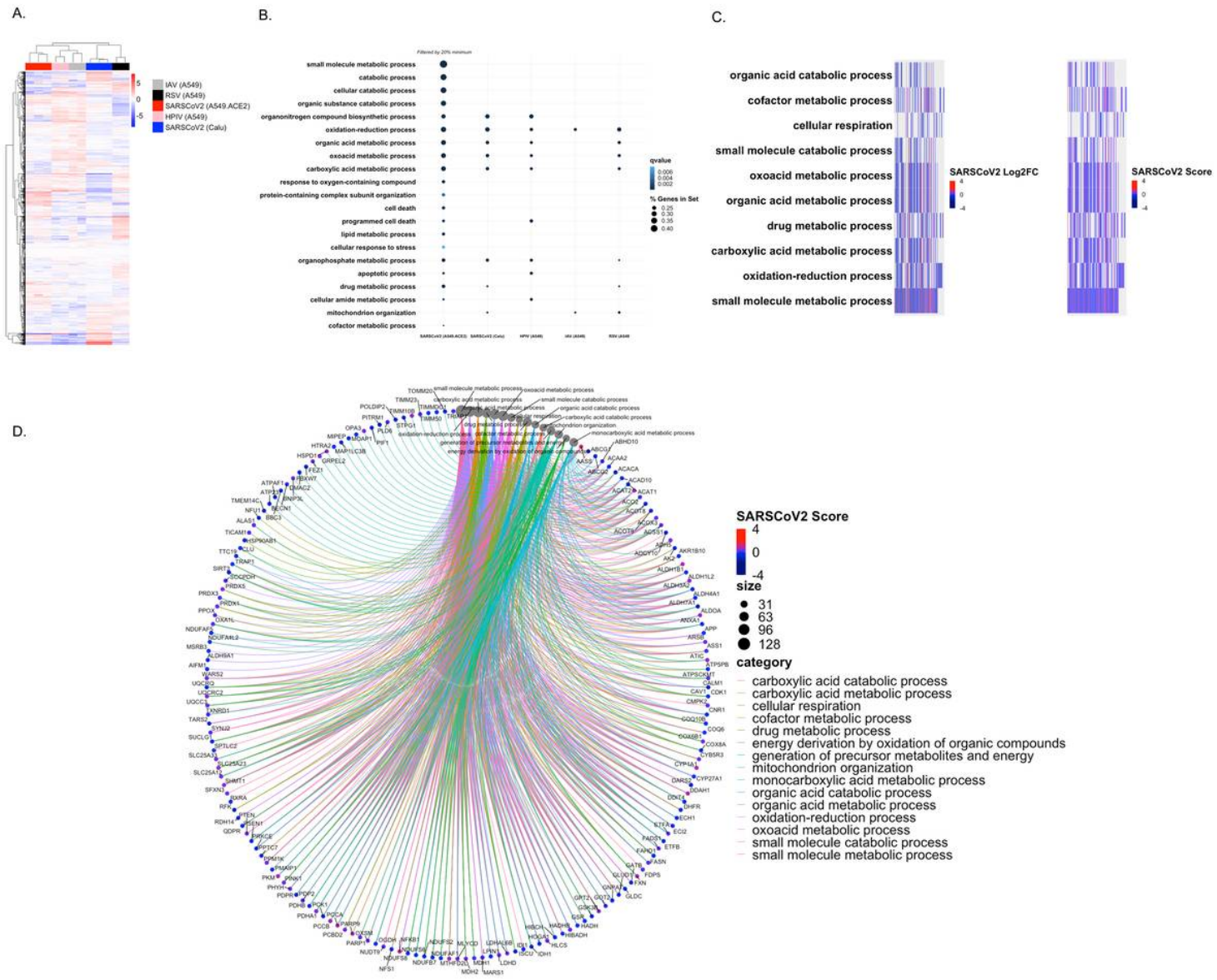

Figure 5

Biological processes affected by NEM expression in cell lines. Hierarchical clustering of all NEMs separate SARS-CoV-2 from other viruses (A). Top NEM biological processes by >20% gene set enrichment (B). Top NEM biological processes by q value; left panel colors represent log 2-fold change of NEMs after SARS-CoV-2 infection and right panel represents hierarchical clustering SARS-CoV-2 score mean of Calu-3 and A549 from panel A (C). Circos plot illustrating significant NEMs and interconnectedness among biological processes.

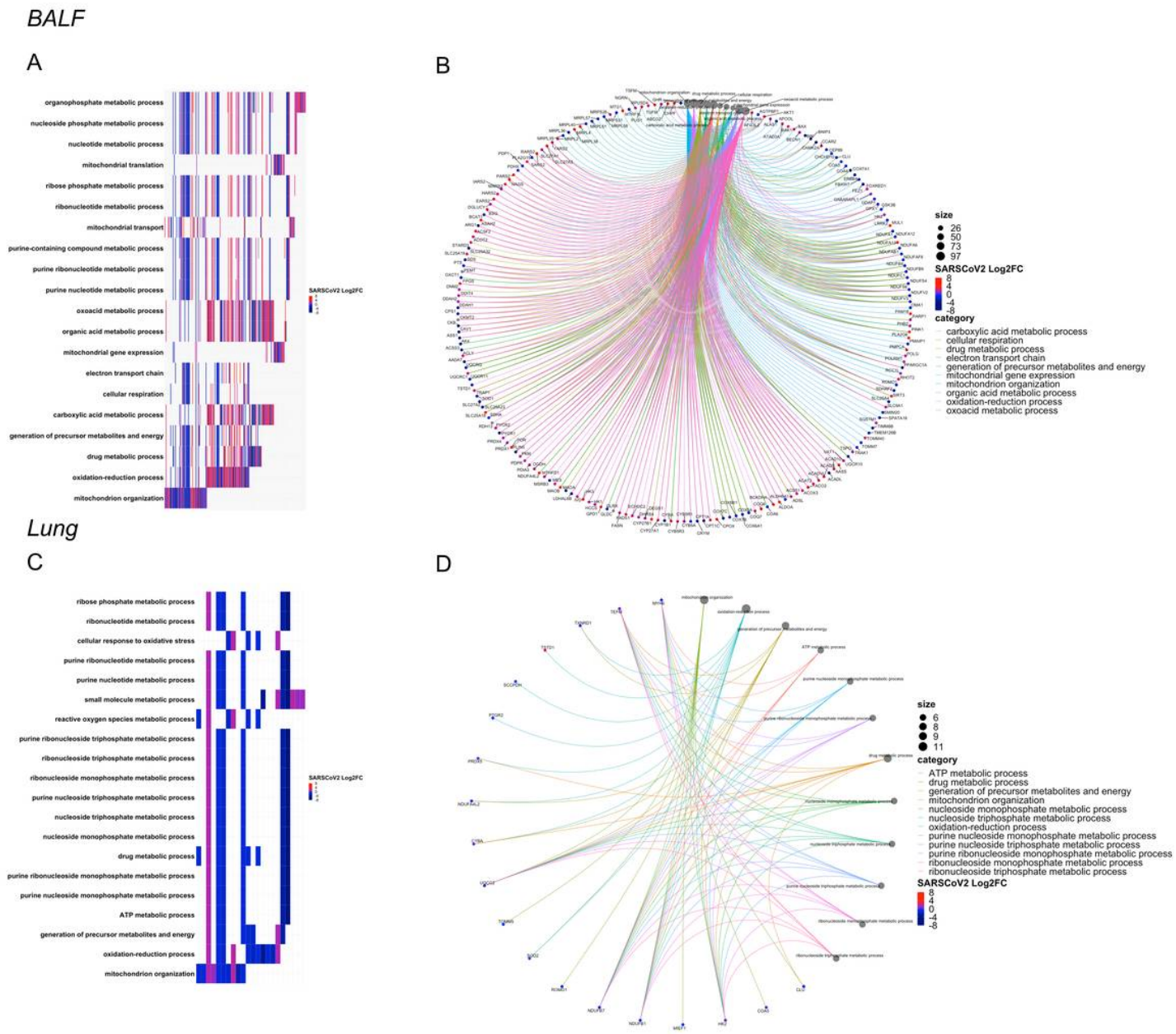

Figure 6

Biological processes affected by NEM expression in clinical. Most significant (by qvalue) NEM-enriched biological processes (A, C) and corresponding genes in circos plot (B,D) with color representing log 2 fold change in BALF and lung, respectively.

Supplementary Files

This is a list of supplementary files associated with this preprint. Click to download.

- mtDNAdegs.xlsx